Failure mechanisms of aluminium foams under compressive loads

E. Sáenz, A. Villate
United Technologies Research Center GmbH, c/o CTA
Parque Tecnológico de Alava, 01510 Miñano, Alava, Spain
I. Garuz , A.M. Irisarri,
Fundacion INASMET, Camino de Portuetxe, 12, 20009 San Sebastian, Spain
G. Rausch, M. Weber
Fraunhofer Institute for Manufacturing and Advanced Materials (IFAM)
Wiener Strasse 12, 28359 Bremen, Germany

Abstract

The purpose of this paper is the investigation of the major failure mechanisms of aluminum foams, which were obtained by powder metallurgical route, under compressive loads. The study was focused on two commonly aluminum alloys AlMg1Si or A 6061 and AlSi12. Due to the fact that the failure mechanisms strongly depend on the density and the macrostructural properties of the material, the mechanical properties must be correlated to the structural properties. Therefore, macrostructural investigations were used as a basis to establish the correlation between structural and mechanical properties.
This was done with a commercially available image analysis system. The average cell size, the cell size distribution and the cell density (number of cells/area) were obtained. In order to evaluate the influence of foaming direction on the cell morphology cross sections parallel and perpendicular to the foaming direction were prepared.
For the characterization of the mechanical compression properties the compressive or upper yield strength (UYS), the densification strain (eD), the energy absorption (Ea) and the efficiency (Eff) were obtained. Furthermore, the failure behavior of the samples was in-situ observed with a video camera and continuously recorded during the test.

1 Introduction

The interesting combination of properties (light weight, good energy absorption, low thermal conductivity, recyclability, etc) of metal foams have spurred new process developments and optimization with the goal to obtain materials with an optimized relation between material's properties and costs [1]-[6]. One of the main advantages of the powder metallurgical route is the production of 3D near-net shape products which allows time reduction on the process and reduction of scrap material [7], [8].
Because most possible applications of metal foams involve compression loading this work is focused on the study of two new metal foams under uniaxial compression (A6061 and AlSi12).

J. Banhart, M.F. Ashby, N.A. Fleck: *Metal Foams and Porous Metal Structures.* © MIT Verlag (1999)

2 Experimental method

2.1 Aluminum foam manufacturing and sample preparation

The aluminum foams were prepared by the powder metallurgical route following the parameters described by Fraunhofer- IFAM Researcher's patents [9], [10]. The powders were mixed with a foaming agent (TiH_2), then the mixture was compacted or extruded to obtain rectangular sheets or cylindrical foamable semi-finished products. This product is inserted into a mould which is heated up to temperatures close to the Al alloy melting point, the TiH_2 decomposes and H_2 gas is released and causes the expansion. Finally the foam occupies the whole mould producing a near-net shape product.
For this study 80x80x200 mm bricks of AlMg1Si (A 6061) and AlSi12 alloys with an average density of 0,55 and 0,57 g/cm^3, respectively, were supplied.
In order to clearly define the three geometric directions according to the foaming direction, the three letters S, L and T were chosen. The foaming direction is indicated with S. L-direction is perpendicular to S and coincides to the largest brick dimension. T is perpendicular to S and L. The plane spread between two directions is indicated with the corresponding letters of the two directions, e.g. TS, LS (see Figure 1).
Three cubic specimens of 60x60x60 mm were cut out from the center of each brick (MIDDLE, L1 and L2) and the upper and lower skin areas were removed, too, by spark erosion. This process avoids cell and surface damage and the obtained samples have good tolerances and parallel surfaces. This allows uniform load distribution over the entire sample surface during the compression test.
Figure 1 shows the area from which the cubic samples were obtained and the density (ρ) variation on both alloys. It can be observed that:

- Density of the MIDDLE is higher than L1 and L2 samples.
- Density of lower skin area is the highest on both alloys , nevertheless on A 6061 alloy is quite similar to the density of upper skin area.
- AlSi12 has the maximum relative density variation $\Delta\rho/\rho_{(avg)}$, that is (highest – lowest density)/average density, and maximum relative standard deviation $S(\rho)/\rho_{(avg)}$.
- The density of cubic samples was around 78% and 90% of total brick density on alloys A 6061 and AlSi12, respectively. This relation could changes depending on brick-sample dimensions and sampling.

2.2 Compression test

The cubic specimens were tested according to the compression test standard prepared in the METEOR project [11] based on ASTM C 367, D1621 and DIN53421 standards [12]-[14]. The main testing parameters are:
The load was applied by rigid load plates, which maintain their initial alignment throughout the entire loading process.

- The cross head speed applied was 10% of sample thickness per minute
- The compressive strain was obtained by measurement of load plates displacements

Figure 2 shows the different results that could be obtained from each compression test. For this paper the compressive or Upper Yield Strength (UYS), collapse plateau (C) and densification slopes (D), the Energy Absorption and Efficiency until 50% strain ($Ea_{50\%}$ $\eta_{50\%}$), and the compressive strength at 50% strain ($\sigma_{50\%}$) were shown. The results are the average of all samples tested (4 per direction and per alloy). Figure 3 shows a typical compressive stress-strain curve for the three testing directions (L, S, T) on studied samples, the specimen density is indicated in brackets.

The tests were carried out in an INSTRON 5500R universal testing machine, a video recording was done in order to analyze the failure sequence.

2.3 Cell structure characterization

In order to have more information about the material characteristics a cell structure characterization was carried out. The cell size distribution along two perpendicular cross-sections (TS and LS) through two bricks per alloy was analyzed. The study was carried out on the complete sample (100%) and was described previously [15]. A total of six samples of 80x80x10 mm were obtained from two different bricks per alloy (3 on LS plane and 3 on TS plane).
Samples were cut by spark erosion in order to avoid cell wall damage and embedded in black resin. These mounted specimens were then ground and polished. The image of the polished cross-section was acquired by a TV camera and later processed to obtain an enhanced image.
The parameters obtained were average cell size or equivalent diameter (m), its standard deviation (σ), cell density (NC/cm^2) or number of cells per unit area and shape factor. The software used to analyze the images was Optimas 6.1 [16].

3 Results and discussion

3.1 Compression properties

The average compression test results are shown in Table I. In order to include the influence of density on compression results specific values (property divided by density) are also shown.

Table I: Average compression test results

Alloy	Direc-tion	UYS (MPa)	UYS spec (MPa.m3/kg)	C (MPa)	C spec (MPa.m3/kg)	$\sigma_{50\%}$ (MPa)	$Ea_{50\%}$ (MJ/m3)	$Ea_{50\%}$ (KJ/kg)	$\eta_{50\%}$ (%)	D (MPa)	D spec (MPa.m3/kg)	eD (%)
A 6061 (AlMg1Si)	S	3,57	0,008	17	0,039	11,36	3,22	7,32	57	98	0,22	61
	L	6,44	0,015	15	0,037	12,46	4,2	9,92	67	101	0,24	61
	T	6,18	0,014	17	0,039	13,51	4,41	9,86	66	98	0,22	59
AlSi12	S	6,29	0,012	18	0,036	14,94	4,88	9,75	65	93	0,19	59
	L	6,11	0,011	19	0,040	15,28	5,54	11,18	72	93	0,19	59
	T	4,02	0,007	24	0,045	16,33	5,19	9,60	65	86	0,16	67

The following conclusions could be drawn:

- Absolute values and specific results give in general similar comparative information.
- In general, in both materials, the compressive strength increases if the compressive strain increases. As an example, the compression strength at 50% ($\sigma_{50\%}$) is around two times the UYS.
- Both materials show a scattering of the UYS, e.g. the lowest UYS on A6061 and AlSi12 are 44% and 36% lower than the highest values; however when $Ea_{50\%}$ is analyzed lower differences were found (26% and 12% on A6061 and AlSi12 respectively).
- The samples who have the lowest UYS usually have the highest collapse slope C and densification strain eD, which was over 59% on both alloys.
- The densification slope (D) tends to be similar between the three testing direction in each alloy.
- The lowest $Ea_{50\%}$ and Efficiencies were obtained on foaming (S) direction.

3.2 Structural analysis

Table II: Millistructure average results

Alloy	Plane	m (mm)	σ (mm)	NC/cm²	Shape factor	95% of cell size Lower than
A 6061 (AlMg1Si)	LS	1,4	1,2	20,29	0,675	3,8 mm
	TS	1,4	1,2	22,03	0,676	3,6 mm
AlSi12	LS	1,2	0,9	27,57	0,691	3,1 mm
	TS	1,2	0,9	28,16	0,696	3,1 mm

Figure 4 shows typical cell size distribution as a function of cell density, as well as the accumulated distribution. Table II shows the average results obtained after characterization of all the samples. The following conclusions could be obtained:

- All samples have some big cells, which are 6 or 7 times bigger than the average cell size. Moreover, in some compression samples big cavities were observed, too. These big cells or cavities can be considered as material defects, this characteristic justifies the high σ values.
- Similar average cell size (m) values were obtained between all cross sections of each alloy. The low shape factor values confirm that on average the cell shape is not spherical, however there are areas where more spherical cells can be observed.
- Higher values of NC/cm^2 and shape factor were obtained on AlSi12 than on A 6061 material, moreover, 95% of cells have sizes lower than 3,1 mm and 3,7 mm on mentioned alloys. This means that higher densities are related to lower average cell sizes and higher NC/cm^2.

Table III: Density and cell size per sections

Alloy	Section	ρ (g/cm³)	m (mm)
A 6061 AlMg1Si	Upper	0,53	1,16
	Middle	0,38	1,43
	Lower	0,35	1,55
AlSi12	Upper	0,45	1,08
	Middle	0,47	1,30
	Lower	0,40	1,28

Table III shows the density variation between different samples (40x40 mm, 22mm height). These values were obtained when cubic samples were divided in three similar parts and ordered following the foaming direction. Thus, "upper section" means the area located in the top of the sample whereas "lower section" means the area located in the bottom surface. Alloy AlSi12 shows better material distribution per section than A6061, where the highest densities are located in the upper section. It is observed that lowest densities not always mean highest cell size.

3.3 Failure mechanism

After the analysis of the videos obtained during the compression tests, no preferred area or region where the failure starts could be determined. Many factors, like mould shape, preformed material distribution inside the mould, foaming conditions, alloy, foam defects, testing direction, sample characteristics, etc. make the determination of the area where the failure starts very difficult. Some studies focused on melt route metal foams over specific cross sections demonstrate that the failure started as a pure cell crushing [17]. Other models use the honeycombs behavior under compressive load as a reference [18]. According to the observations made during this study, the failure process is a mixed mechanism of crushing and shearing of cells, because of the interaction of factors like inhomogeneous density distribution, cell size, cavities, etc.

Figure 5 shows a typical mechanism of failure on material A 6061 tested in T and L directions respectively. The failure starts in a non linear band, that means that the surface of failure is not parallel to the load plates surfaces and follows an intricate 3D surface where cells fail by crushing and shearing, probably due to the effect of areas with higher resistance (same as above) which act as indenters into weaker areas.

In other samples a more uniform failure was detected at initial stages, starting by pure crushing in a plane parallel and close to one load plate and progressing similarly, layer by layer, until stronger and lower areas were contacted, hence failure progress continued in the same way as described previously.

4 Conclusions

In the initial stages the failure mechanism is dominated by a crushing-shearing cell failure associated to the interaction between non-uniform material and cell size distribution and material's defects (cavities). These characteristics do not allow an easy estimation on where the material failure starts and how it will progress along the sample.
As the compressive strain increases, the mechanism tends to be similar to multiple indenters penetrating in the material, where the indenters are associated to material's regions or areas with more compression resistance and probably associated to highest local densities.

5 Acknowledgments

The authors gratefully acknowledge the millistructure characterization of Guillermo Caruana of CENIM, Spain.
The research work has been carried out within the framework of the European Commission's „Industrial and Materials Technologies" (Brite EuRam III) multiannual (94-98) program for R&D. The authors gratefully acknowledges the collaboration of all partners of the METEOR project „Light-weight Metal Foam Components for the Transport Industry" (Contract BRPR-CT96-0215 - BriteEuRam project BE96-3018).

6 References

[1] M. Yu, J. Banhart: Overview: Properties of Metal Foams. In "Metal Foams", Hrsg: J. Banhart und H. Eifert, Verlag MIT, Bremen (1998)
[2] J. Banhart, W. Brinkers: Fatigue behaviour of aluminium foams. J. Mat. Sci. Let. **18** (1999), 617-619
[3] G.J. Davies; S. Zhen. J. Mat. Sci. 18, 1899 (1983).
[4] J. Banhart, J. Baumeister, M. Weber: Aluminium Foams for Automotive Applications, 29th Int. Symp. Auto. Tech. & Automotive (ISATA), Conference Paper No. 96NM006. Florence, (1996)
[5] L. Lorenzi, A. Fuganti, E. Todaro, E. Fossat: Aluminium Foam Applications For Impact Energy Absorbing Structures. SAE Technical Paper Series No. 970015 (1997)
[6] J.T. Beals; M.S.Thompson. UTRC internal report, (1996)
[7] J. Banhart: Production methods for metal foams. In "Metal Foams", Hrsg: J. Banhart und H. Eifert, Verlag MIT, Bremen (1998)
[8] J. Banhart, J. Baumeister: Overview: Production methods for metallic foams. MRS Symp. Proc., Ed.: D. Schwartz et al. (1998)
[9] J. Baumeister. US Patent 5 151 246 (1992). European Patent No. 0460392A1 (1996)
[10] J. Baumeister, J. Banhart, M. Weber, German Patent DE 44 26 627 (1997)
[11] Brite-EuRam Project METEOR (BE96-3018): Detailed Description of experimental testing procedure, 1997
[12] ASTM C 365-57 (reapproved 1998), Flatwise compressive strength of sandwiches cores
[13] ASTM D1621-73 (reapproved 1979), Compressive properties of rigid cellular plastics
[14] DIN 53421, Testing of rigid cellular plastics
[15] E. Sáenz, P. Baranda, J. Bonhomme, Mat. Res. Soc. Symp. Proc., Vol 521, 83 (1998)
[16] Optimas 6.1, software. Optimas Corporation. Washington, 1996.

[17] H. Bart-Smith, A. Bastawros et al, Mat. Res. Soc. Symp. Proc., Vol 521, 71 (1998)
[18] L.J. Gibson, M. Ashby, Cellular Solids: Structure and Properties, Cambridge University , Cambridge, 2nd edition, (1997).

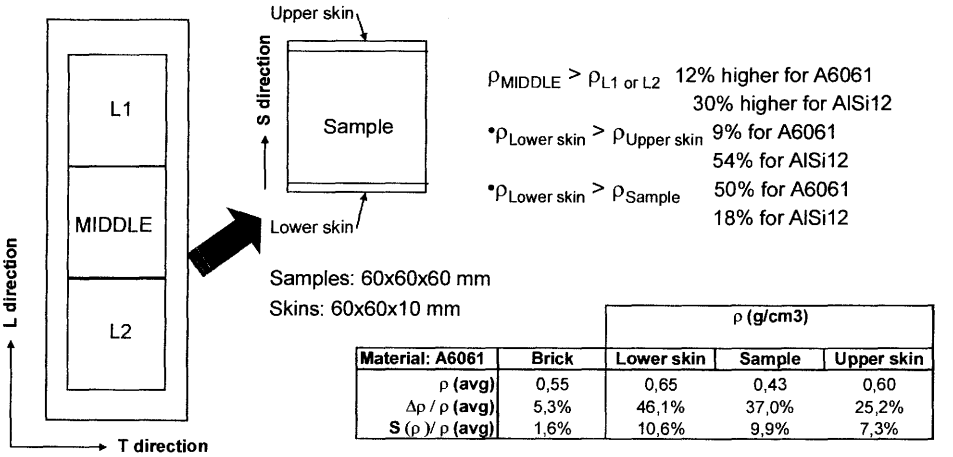

		ρ (g/cm3)		
Material: A6061	**Brick**	**Lower skin**	**Sample**	**Upper skin**
ρ (avg)	0,55	0,65	0,43	0,60
Δρ / ρ (avg)	5,3%	46,1%	37,0%	25,2%
S (ρ)/ ρ (avg)	1,6%	10,6%	9,9%	7,3%
Material: AlSi12				
ρ (avg)	0,57	0,69	0,51	0,45
Δρ / ρ (avg)	9,5%	44,7%	41,1%	46,8%
S (ρ)/ ρ (avg)	2,9%	10,1%	14,5%	14,1%

Figure 1: Material sampling and density comparison

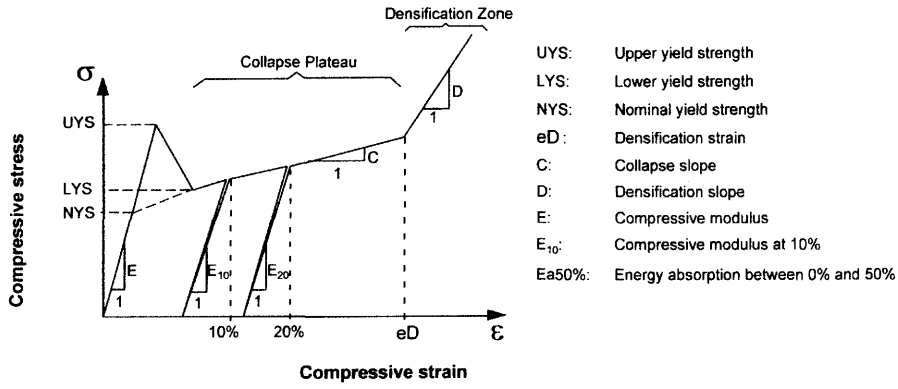

Figure 2: Schematic stress-strain curve of a compression test.

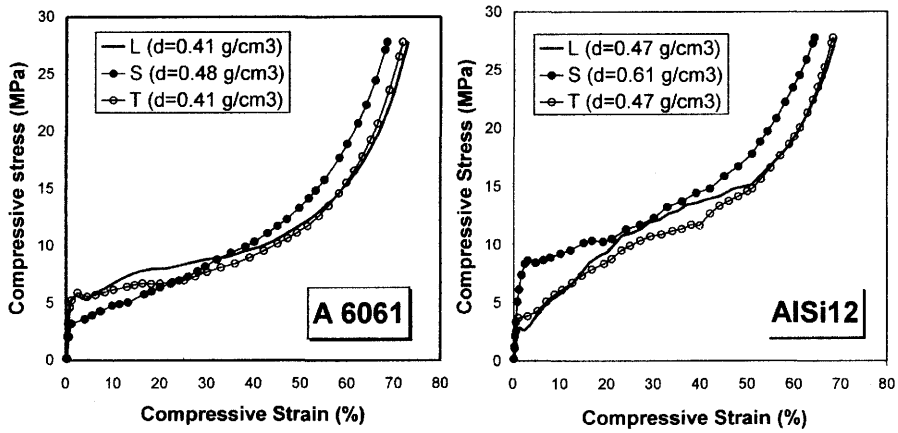

Figure 3: Compression tests curves of A 6061 and AlSi12 alloys.

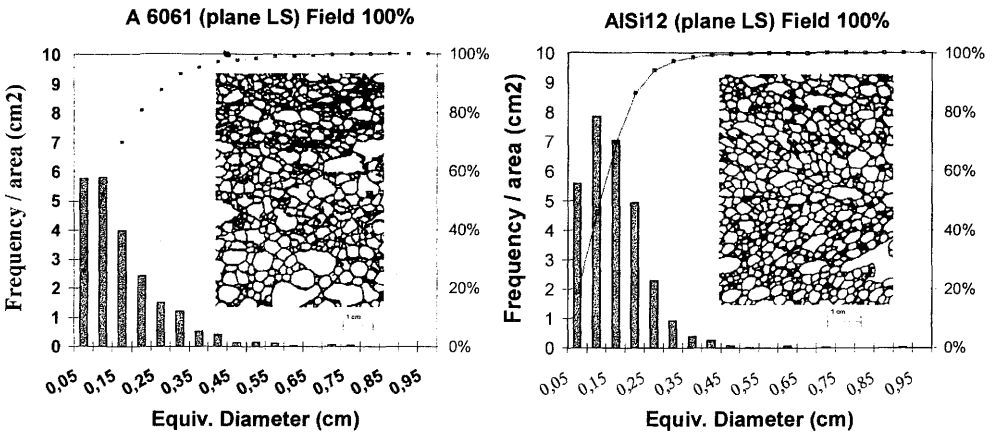

Figure 4: Typical cell size (Equiv. Diameter) vs. Cell density distribution. Typical A6061 and AlSi12 millistructures.

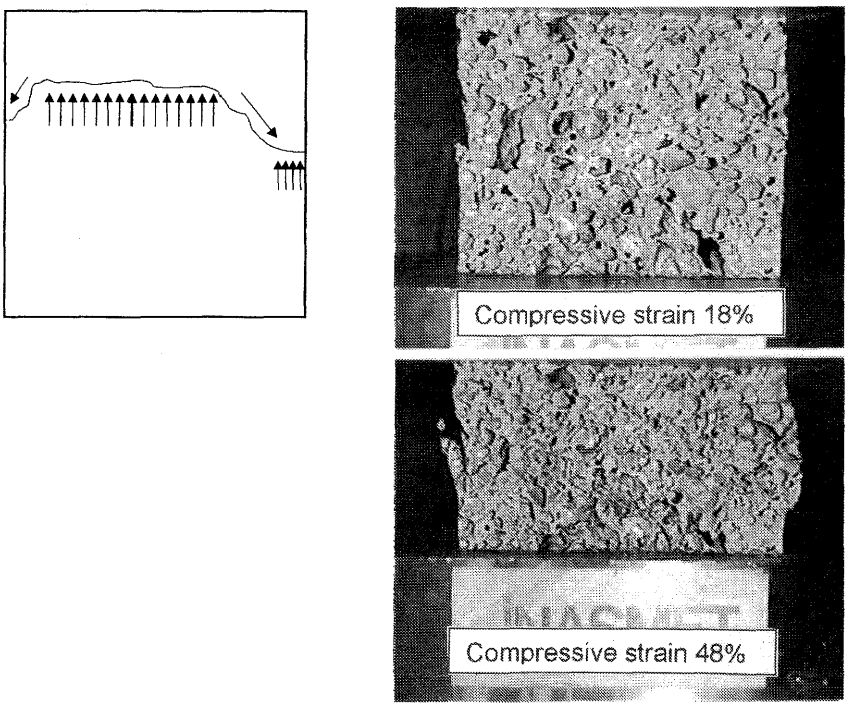

Figure 5: Typical failure mechanism during compressive loading (tested in L direction): Compression loads produce initial local cells crushing and shearing. Deformation planes (left picture) are formed and samples increase width due to shear effects.